Supplementary Information Appendix

Temperature dependence of protein folding kinetics in living cells

Minghao Guo, Yangfan Xu, and Martin Gruebele

1. Faster stepping, sample temperature and reversibility When using the fast step method to measure thermodynamic equilibrium, the simple laser power steps illustrated in Figure 1 of the main text are sufficient. However, the temperature takes ≈2 s to equilibrate. Another ≈2 seconds are needed for FRET-PGK conformational equilibrium. We can accelerate this process by applying an overshoot at the beginning of each step. A smaller overshoot can be used to produce a square-shaped temperature profile, allowing kinetics and thermodynamics (via kinetic amplitude, ref. S3) to be collected simultaneously. An even higher transient overshoot accelerates equilibration further, allowing the fastest thermodynamic measurements. This method makes the sample go to the next thermodynamic data point in only 2 s. Figure S1 shows how the laser power and temperatures increases in the even faster method with initial spikes.

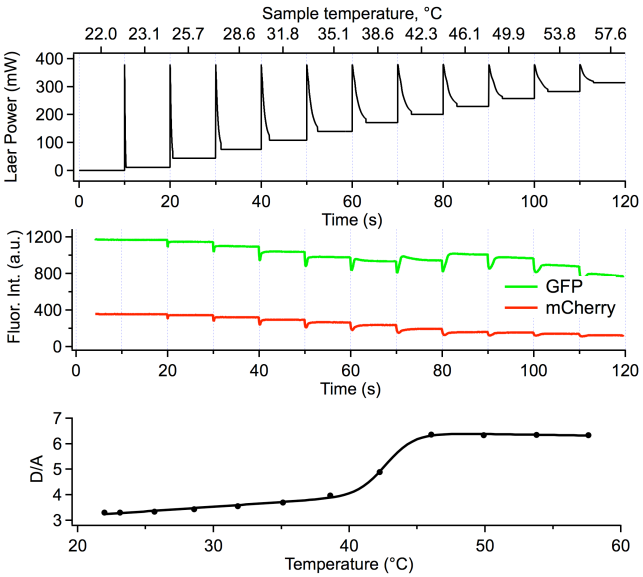

Figure S1. Overshoot stepping for fast acquisition of thermal profiles. Top: Laser power as a function of time, and temperature at the end of each step. Middle: FRET-PGK response in the green and red camera channels. Bottom: thermal denaturation profile. Note that 10 s were used here for each step to show equilibration. Equilibration was complete after ≈2 s for each step.

We checked the reversibility of the fast thermodynamics method over the temperature range of interest *in vivo* and *in vitro*. Stepping the power upwards heats the sample to 48 °C before downward stepping decreases the sample temperature back to room temperature (Figure S2). The intensities at the beginning and end lie within ±3% after 200 seconds exposure. (Slight photobleaching reduces the intensity at the end. We also observe a very fast reversible photobleaching before the steps are started at t=0, hence the intensity at the end is sometimes slightly larger than at t=0, but not larger than the initial intensity.) An alternative approach to prevent photobleaching is to turn on the LED only at the very end of each step for measurement. This produces (again within 3%) the same final fluorescence intensity as always keeping the LED on, providing that the LED power is low enough.

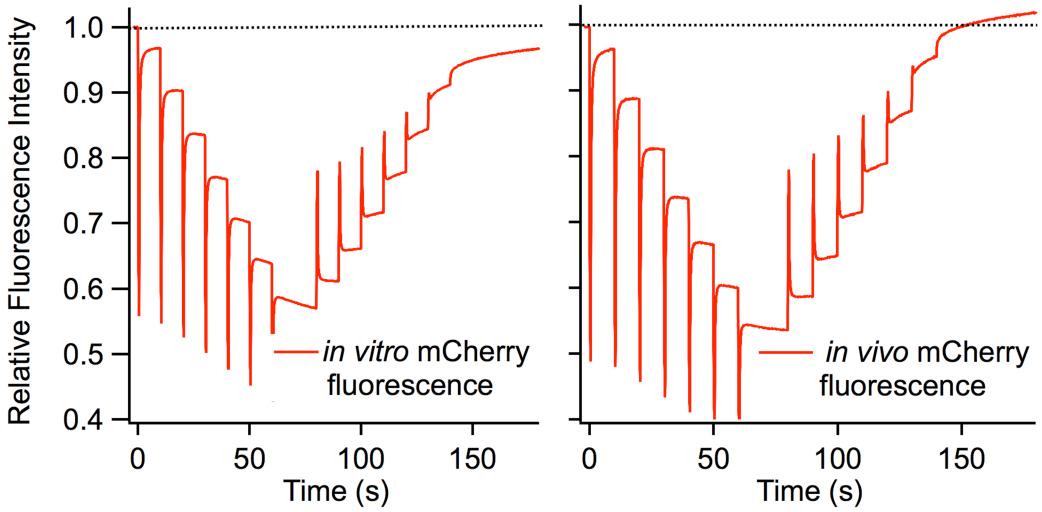

Figure S2. Reversibility of mCherry fluorescence intensity *in vitro* and *in vivo* heated by overshoot stepping from 22 to 48 °C and back. Stepping reverses at 70 seconds. At higher temperatures (e.g. Figure 1 in main text) irreversible aggregation is observed, yielding significant loss of fluorescence intensity.

2. Kinetics fitting The kinetics traces in term of $D(t)$-$a\mathrm{A}(t)$ have a non-zero slope at the end due to photobleaching. The photobleaching baselines are obtained by fitting the final 4 s of the kinetics traces after the system equilibrates to a straight line. The baseline subtracted traces are then fitted to stretched exponentials to yield k_{obs} (see main text).

Effective two-state rate coefficients for folding and unfolding were calculated from K_{eq} and k_{obs} as

$$k_f = k_{obs} f_{native} = k_{obs} K_{eq} / (1 + K_{eq}) \quad [S1]$$

and

$$k_u = k_{obs} f_{unfolded} = k_{obs} / (1 + K_{eq}) . \quad [S2]$$

K_{eq} is the equilibrium constant extracted from the thermodynamic measurement by fitting eq. [1] of the main text to thermal melts such as Figure 1B. f are the fractions of native and unfolded states used to calculate the thermal melting curve by assuming the observed signal is a sum of the native and unfolded signals, each signal being represented by a linear baseline to account for temperature-dependent quantum yields. k_{obs} is the observed rate coefficient extracted from kinetics data such as Figure 2 by fitting a stretched exponential function as described in the main text. k_f and k_u are then fitted to the effective two-state rate model (analogous to eq. [1] in the main text):

$$\ln(k_0 / k_{u,f}(T)) = \frac{\Delta G^{\dagger}_{u,f}(T)}{RT} = \frac{1}{RT}\left[\Delta H^{\dagger}_{u,f}(T_m) - T\Delta S^{\dagger}_{u,f}(T_m) + \Delta C^{\dagger}_{p;u,f}\left(T - T_m + T\ln(T_m / T)\right)\right]. \quad [S3]$$

The subscript "u" refers to the unfolding reaction, "f" to the folding reaction. This kinetic two-state fitting model and eq. [1] in the main text assume that the heat capacity for folding is a constant. The rate prefactor k_0 is a function of solvent viscosity such that

$$k_0 = (10\,\mu\text{s})^{-1}\left(\frac{\eta(22\ ^{\circ}\text{C})}{\eta(T)}\right)^{\gamma}. \quad [S4]$$

η is the solvent viscosity. $(10\ \mu\text{s})^{-1}$ is an estimate of the barrier-free rearrangement rate at 22 °C (see main text). The viscosity depends on temperature as $\eta(T) = 0.226 + 1.0723e^{-(T-10^{\circ}C)/33}$ (ref. S1). γ determines how much the viscosity affects the prefactor (ref. S2). γ=1 was chosen for fits of the experimental data.

3. Kinetic fitting results The folding and unfolding rates were fitted to the two-state model described above and in the main text. Table S1 shows the resulting fitting parameters. Since k_f and k_u were derived using K_{eq}, the folding rate, unfolding rate and thermal denaturation parameters are of course not independent. The thermal denaturation parameters ΔH, ΔS and ΔC_p in eq. [1] of the main text can be obtained from the appropriate differences of the kinetic fitting parameters because

$$\Delta G(T) = \Delta G_f^{\dagger}(T) - \Delta G_u^{\dagger}(T)\,. \qquad \text{[S5]}$$

Table S1. The fitted results of $\Delta H_{f,u}^{\dagger}$, $\Delta S_{f,u}^{\dagger}$ and $\Delta C_{p;f,u}^{\dagger}$ for the six cell of which the temperature dependent kinetics shown in Figure 4 in the main text. T_m has units of ºC. $\Delta H_{f,u}^{\dagger}$ has unit of kJ/mol. $\Delta S_{f,u}^{\dagger}$ and $\Delta C_{p;f,u}^{\dagger}$ have units of kJ/mol/K.

	in vitro	Cell a	Cell b	Cell c	Cell d	Cell e	Cell f
T_m	39.9±0.5	42.3±0.6	42.1±1.4	43.1±3.5	41.8±2.3	43.0±0.4	42.5±0.3
$\Delta H_f^{\dagger}$	-333±20	-376±82	-380±20	-357±11	-520±82	-414±15	-421±44
$\Delta S_f^{\dagger}$	-1.18±0.06	-1.31±0.26	-1.33±0.06	-1.26±0.04	-1.77±0.26	-1.43±0.05	-1.45±0.14
$\Delta C_{p;f}^{\dagger}$	-48±9	-97±35	-96±16	-79±9	-40±39	-69±11	-39±26
$\Delta H_u^{\dagger}$	337±24	290±75	397±23	428±12	227±80	331±17	323±50
$\Delta S_u^{\dagger}$	0.96±0.08	0.80±0.24	1.14±0.07	1.23±0.04	0.60±0.25	0.93±0.05	0.90±0.16
$\Delta C_{p;u}^{\dagger}$	-38±8	-90±29	-87±16	-85±9	-25±33	-62±10	-23±24

4. Hierarchical free energy landscape A minimal three-state FEL of PGK folding was investigated. The FRET efficiencies of the U, I and N states are 0.14, 0.195 and 0.25, respectively, and were assumed to be temperature-independent. At a melting temperature of 313 K, the free energies of all three states are zero. The barriers $\Delta G_{UI}^{\dagger}$ and $\Delta G_{IN}^{\dagger}$ were set to 12.68 and 11.46 k_BT to produce stretched exponential kinetics of $\tau \approx 2$ *s,* $\beta \approx 0.8$. The simulation was performed at temperatures from 298 K to 328 K. All the free energies were tuned as $\Delta G^{(1)} = G^{(1)}$ $\varphi\,(T\text{-}T_m) = 0.5\ k_BT/K\ \varphi\,(T\text{-}T_m)$, where φ=0, 0.25, 0.5, 0.75 and 1 for G_U, $\Delta G_{UI}^{\dagger}$, G_I, $\Delta G_{IN}^{\dagger}$ and G_N. Rate coefficients were calculated as in eq. [S3] with γ=0 (constant prefactor). Simulations of relaxation after a 4 °C T-jump were performed following Eq. 2 in the main text. The resulting concentrations as a function of time were converted to simulated $D(t)$ and $A(t)$ using the FRET efficiencies given above. The simulated data was then fitted to stretched exponentials to yield β and k_{obs}. The final signals at each temperatures are used in calculation of equilibrium constant $K_{eq}(T)$. β was discarded, while k_{obs} and K_{eq} were converted to k_u and k_f and fitted to the effective two-state model just like the experimental data. The fitted two-state T_m agrees with the actual input T_m = 313 K of the FEL within 0.2 degrees.

The basic form of the FEL discussed above did not yield rate vs. temperature plots that looked exactly like the experimental ones (compare Fig. 4 with Figure 6A). Two modifications

of the rate coefficients computed from the FEL yielded the best agreement. An alternative set of activation barriers with an additional quadratic term $\Delta G^{(2)} = G^{(2)}\ \varphi\ (T-T_m)^2 = 0.008\ k_B T/K^2\ \varphi\ (T-T_m)^2$ was also used to compute kinetics, as shown in Figure 6C and 6D. Finally, a viscosity dependence like eq. [S4] was also added to the simulated rate coefficients (Figure 6B and 6D). The larger γ is, the steeper the temperature dependence of k_0 is, which produces a larger tilt of the folding and unfolding rates curves in Figure 4 of the main text. Figure S3 compares the fit without a viscosity dependence, to the fit with a γ=0.6 viscosity dependence often used in the literature for proteins (ref. S2). As expected, the γ=0.6 result is intermediate between the γ=0 and 1 results shown in Figure 6 A and B of the main text.

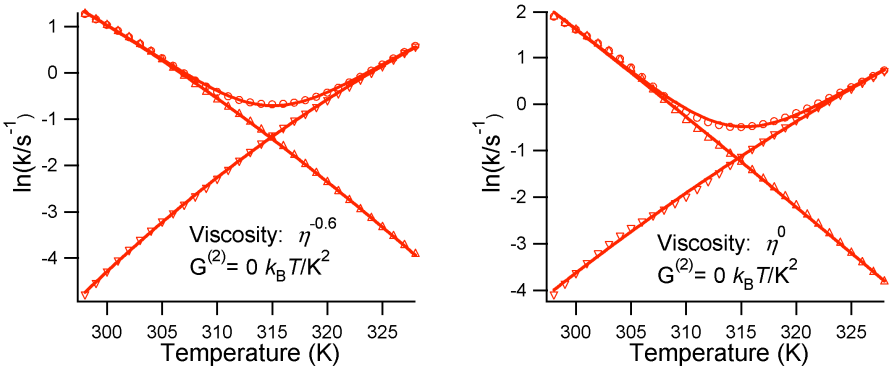

Figure S3. Comparison of minimal hierarchical three-state model with (γ=0.6) and without (γ=0, same as in main text) fractional bulk solvent viscosity dependence.

5. References

S1. Denos S (2009) *Studies of protein folding on membranes and in crowded environments and bridging the research-teaching gap in K-12 science.* (Doctoral dissertation, University of Illinois), pp85.

S2. Hagen SJ (2010) Solvent viscosity and friction in protein folding dynamics. *Curr Protein Pept Sci* 11: 385-395.

S3. Girdhar K, Scott G, Chemla YR, Gruebele M (2011) Better biomolecule thermodynamics from kinetics. *J Chem Phys* 135: 015102.